

Thermal Hall Effects of Spins and Phonons in Kagome Antiferromagnet Cd-Kapellasite

Masatoshi Akazawa¹, Masaaki Shimozawa^{1,2}, Shunichiro Kittaka^{1,3},
Toshiro Sakakibara¹, Ryutaro Okuma^{1,4}, Zenji Hiroi¹, Hyun-Yong
Lee^{1,5}, Naoki Kawashima¹, Jung Hoon Han⁶, and Minoru Yamashita^{1*}

¹*The Institute for Solid State Physics,*

The University of Tokyo, Kashiwa, 277-8581, Japan

²*Graduate School of Engineering Science,*

Osaka University, Toyonaka, 560-8531, Japan

³*Department of Physics, Chuo University,*

Kasuga, Bunkyo-ku, Tokyo 112-8551, Japan

⁴*Okinawa Institute of Science and Technology*

Graduate University, Kunigami-gun, 904-0495, Japan

⁵*Division of Display and Semiconductor Physics,*

Korea University, Sejong, 30019, Korea and

⁶*Department of Physics, Sungkyunkwan University, Suwon 16419, Korea*

(Dated: June 7, 2022)

Abstract

We have investigated the thermal-transport properties of the kagome antiferromagnet Cd-kapellasite (Cd-K). At low temperatures, the longitudinal thermal conductivity κ_{xx} was strongly suppressed in the magnetic field, suggesting a large spin contribution κ_{xx}^{sp} . Clear thermal Hall signals were observed in the spin liquid phase in all Cd-K samples. We find a large sample dependence of the magnitude of the thermal Hall conductivity κ_{xy} of Cd-K, of which the peak increases almost linear to κ_{xx} . On the other hand, the temperature dependence of κ_{xy} is similar in all Cd-K samples and shows a peak at almost the same temperature of the peak of the phonon thermal conductivity κ_{xx}^{ph} which is estimated by κ_{xx} at 15 T. These results indicate the presence of a phonon thermal Hall κ_{xy}^{ph} in Cd-K. In addition to κ_{xy}^{ph} , we find that the non-linear field dependence of κ_{xy} at low temperatures indicates the presence of a spin thermal Hall κ_{xy}^{sp} in Cd-K. Remarkably, both κ_{xy}^{ph} and κ_{xy}^{sp} disappear in the antiferromagnetic ordered phase at low fields, showing that κ_{xy}^{ph} alone does not exhibit the thermal Hall effect. A high field above ~ 7 T induces κ_{xy}^{ph} , concomitantly with a field-induced increase of κ_{xx} and the specific heat. These results demonstrate that the spin liquid state in the Cd-K harbors both κ_{xy}^{sp} and κ_{xy}^{ph} , and suggest a coupling of the phonons to the field-induced excitations as the origin of κ_{xy}^{ph} .

I. INTRODUCTION

The magnetic ground state of a two-dimensional (2D) kagome structure has been attracting tremendous attention because the strong frustration effect caused by the corner-sharing network of the triangles has been expected to suppress the magnetic order even at the absolute zero temperature. Instead of a long-range ordered state, emergence of a quantum disordered state of spins, termed as a quantum spin liquid (QSL), has been shown in the kagome Heisenberg antiferromagnet (KHA) by various numerical calculations¹⁻⁸. A lot of QSLs have been theoretically suggested as the ground state of the KHA such as \mathbb{Z}_2 spin liquids^{2,9,10}, topological spin liquids³, Dirac spin liquids^{4,6-8}, and chiral spin liquids¹¹. These different QSLs are characterized by different elementary excitations. It is thus an experimental challenge to pin down the QSL realized in KHA by clarifying the elementary excitation.

Thermal-transport measurement is a powerful probe to study the elementary excitations in QSLs because it has the advantage of detecting only the itinerant excitations. Therefore, one can avoid effects of localized excitations caused by impurities which are often inevitable in candidate materials¹². Moreover, further detail of the elementary excitation can be studied by investigating the thermal Hall effect. It has been shown that the thermal Hall effect in an insulator is given by the Berry curvature of the elementary excitation as

$$\kappa_{xy} = \frac{k_B T}{\hbar V} \sum_k \sum_n c_2[g(\epsilon_{nk})] \Omega_{nk} , \quad (1)$$

where $c_2[g(\epsilon_{nk})]$ is a distribution function given by the elementary excitations of energy ϵ_{nk} and Ω_{nk} is the Berry curvature of the elementary excitations^{13,14}. Therefore, from κ_{xy} measurements, one can study the statics of the elementary excitations (fermions or bosons) as well as the Berry curvature of the corresponding energy bands.

The thermal Hall effect of spins (κ_{xy}^{sp}) has been observed in ferromagnetic insulators, which is well understood as a magnon thermal Hall effect^{15,16}. The spin thermal Hall effect has also been reported in paramagnetic states of kagome¹⁷⁻²⁰, spin ice²¹ and Kitaev compounds²²⁻²⁴. In these frustrated magnets, the paramagnetic phase extends well below the temperatures determined by the interaction energy J , realizing a spin liquid phase in a wide temperature range $T_N \leq T \ll J/k_B$. For κ_{xy} observed in the spin liquid phase of kagome antiferromagnets volborthite and Ca kapellasite (Ca-K), it has been shown that the Schwinger-boson mean field theory (SBMFT)²⁵ can well reproduce both the temperature dependence and the magnitude of κ_{xy} by tuning the two

fitting parameters of the spin interaction energy J and the Dzyaloshinskii-Moriya (DM) interaction D (Ref. ¹⁹). Remarkably, the fitting results of J and D , obtained by the SBMFT fitting to κ_{xy} of both kagome compounds, are close to the values estimated by the temperature dependence of the magnetic susceptibility and that by the deviation of the g factor, respectively. This excellent agreement suggests that the elementary spin excitations in the KHA can be well described by the bosonic spinons of SBMFT.

In addition to the spin thermal Hall effects, the thermal Hall effects of phonons (κ_{xy}^{ph}) have been reported in various compounds^{26–30}. The origin of the phonon thermal Hall has also been extensively studied theoretically^{31–39}. However, the understanding of the phonon thermal Hall effect has been left out in the consideration of spin thermal Hall effect, because the nature of the coupling between phonons and spin fluctuations has remained unclear.

In this Article, we report our thermal-transport measurements of a new kagome compound Cd kapellasite (Cd-K). Previous studies^{40,41} have shown that the spin Hamiltonian of Cd-K is well approximated to a KHA with the spin interaction energy of $J/k_B \sim 45$ K. The frustration effect of the kagome structure suppresses the ordering temperature ($T_N \sim 4$ K) well below J/k_B , realizing a spin liquid phase in a wide temperature range. We find a large contribution of the spins in κ_{xx} which can be essentially turned off by applying a magnetic field. This field-tuning of κ_{xx}^{sp} enables us to find both κ_{xy}^{sp} and κ_{xy}^{ph} in Cd-K. Most remarkably, we find that both κ_{xy}^{sp} and κ_{xy}^{ph} disappear in the AFM phase at low fields. Further, we find that κ_{xy}^{ph} is induced by applying a high field which concomitantly induce additional excitations probed by the specific heat and κ_{xx} . We conclude that Cd-K is a prominent frustrated magnet in which the spin liquid state shows thermal Hall effects of both spins and phonons. The dual nature of the thermal conductivities prompts us to speculate that a coupling of phonons with the field-induced magnetic excitations is taking place to give rise to κ_{xy}^{ph} in this compound.

II. MATERIALS AND METHODS

Cd-Kapellasite $\text{CdCu}_3(\text{OH})_6(\text{NO}_3)_2 \cdot \text{H}_2\text{O}$ is a trigonal compound with space group $P\bar{3}m1$ and lattice constants $a = 6.5449 \text{ \AA}$, $c = 7.0328 \text{ \AA}$ ⁴⁰, in which the magnetic Cu^{2+} ions form an undistorted kagome lattice (Fig. 1 (a)). Cd-K is a structural polymorph of herbertsmithite⁴², in which the Zn ions located between the kagome layer and the site mixings between the Zn and Cu ions¹² allow an inter-layer coupling between the kagome layers. In contrast, in Cd-K, the nonmagnetic

Cd ions are located at the center of the hexagon of the kagome lattice and there is no site mixings in Cd-K because of the larger ionic radii of Cd^{2+} (0.95 Å) than that of Cu^{2+} (0.73 Å)⁴³, realizing a more ideal KHA in Cd-K.

Three magnetic interactions in Cd-K are suggested by the fitting of the magnetic susceptibility as $J/k_B = 45.44$ K, $J_2/J = -0.1$, $J_d/J = 0.18$, where J is the nearest-neighbor interaction, J_2 the next-nearest-neighbor interaction, and J_d the diagonal interaction via the non-magnetic Cd ion (see Fig. 1 (b)). The development of a short-range antiferromagnetic correlation has been shown by the decrease of the magnetic susceptibility below 30 K⁴⁰. The g factors are estimated as $g_a = 2.28$, $g_c = 2.37$ ⁴¹. The lack of the inversion symmetry allows both the in-plane and out-of-plane DM interactions, which has been suggested to cause a negative vector chiral order below the Neel temperature of $T_N \sim 4$ K⁴⁰.

The thermal-transport measurements were performed by the steady-state method as described in Refs. 18–20. One heater and three thermometers were attached to the sample, and then the temperature difference ΔT_x ($\Delta T_x = T_{\text{High}} - T_{L1}$) and ΔT_y ($\Delta T_y = T_{L1} - T_{L2}$) were measured by applying the heat current Q in the kagome plane (Fig. 1 (c)). The longitudinal thermal conductivity κ_{xx} and the thermal Hall conductivity κ_{xy} is derived by

$$\begin{pmatrix} Q/wt \\ 0 \end{pmatrix} = \begin{pmatrix} \kappa_{xx} & \kappa_{xy} \\ -\kappa_{xy} & \kappa_{xx} \end{pmatrix} \begin{pmatrix} \Delta T_x/L \\ \Delta T_y/w \end{pmatrix}, \quad (2)$$

where t is the thickness of the sample, L is the length between T_{High} and T_{L1} , and w is the sample width between T_{L1} and T_{L2} .

We measured κ_{xx} and κ_{xy} of three Cd-K samples (Sample 1, 2, and 3) by using a variable temperature insert (VTI) (2–60 K, 0–15 T). Measurements of Sample 2 were also done in a dilution refrigerator (DR) (0.1–4 K, 0–14 T). The magnetic field was applied along the c axis of the sample. A typical sample is shown in Fig. 1(d). A heat current Q was applied along the direction 1 ($\perp a$ -axis, see Fig. 1(d)) in Samples 1, 2, and the first run of Sample 3 (denoted as Sample 3-1). In the second run of Sample 3 (Sample 3-2), the direction of Q was change to the direction 2 ($\parallel a$ -axis, see Fig. 1 (d)). The specific heat measurement was performed for multiple single crystals by a thermal relaxation method in a temperature range of 0.1–2 K and a magnetic field range up to 14 T.

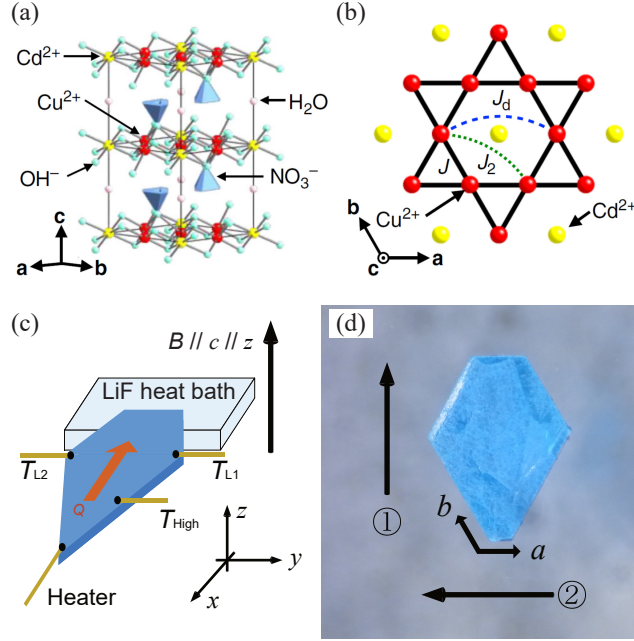


FIG. 1. (a) Crystal structure and (b) top-view of a kagome layer of Cd-K⁴¹. The magnetic interactions between nearest-neighbor, next-nearest-neighbor, and diagonal Cu²⁺ spins are denoted by J (solid black line), J_2 (dotted line) and J_d (dashed line), respectively. (c) Schematic illustration of κ_{xx} and κ_{xy} measurements. A heater and three thermometers (T_{High} , T_{L1} , T_{L2}) were attached to the sample fixed on the LiF heat bath. A heat current Q was applied within the kagome layer and a magnetic field B was applied along the c -axis. (d) A typical crystal of Cd-K. The direction of the heat current for the sample 1, 2, and 3-1 (3-2) is shown by the arrow 1 (2).

III. RESULTS

A. Longitudinal Thermal Conductivity

Figure 2 (a) shows the temperature dependence of κ_{xx} of all Cd-K samples at zero magnetic field. For reference, κ_{xx} of Ca-K¹⁹ is also shown. As shown in Fig. 2 (a), κ_{xx} of all Cd-K samples is about one order of magnitude larger than that of Ca-K. Although the magnitude of κ_{xx} in different Cd-K samples are different in factor of ~ 2 , κ_{xx} of all Cd-K samples show a similar temperature dependence. The temperature dependence of κ_{xx} shows a shoulder-like enhancement around 15 K, which is followed by a hump near T_N and a rapid decrease for $T < T_N$.

The temperature dependence of κ_{xx} at different magnetic fields is shown in Figs. 2 (b)–(f). In all Cd-K samples, a decrease of κ_{xx} by applying the magnetic field was observed below 30 K. This

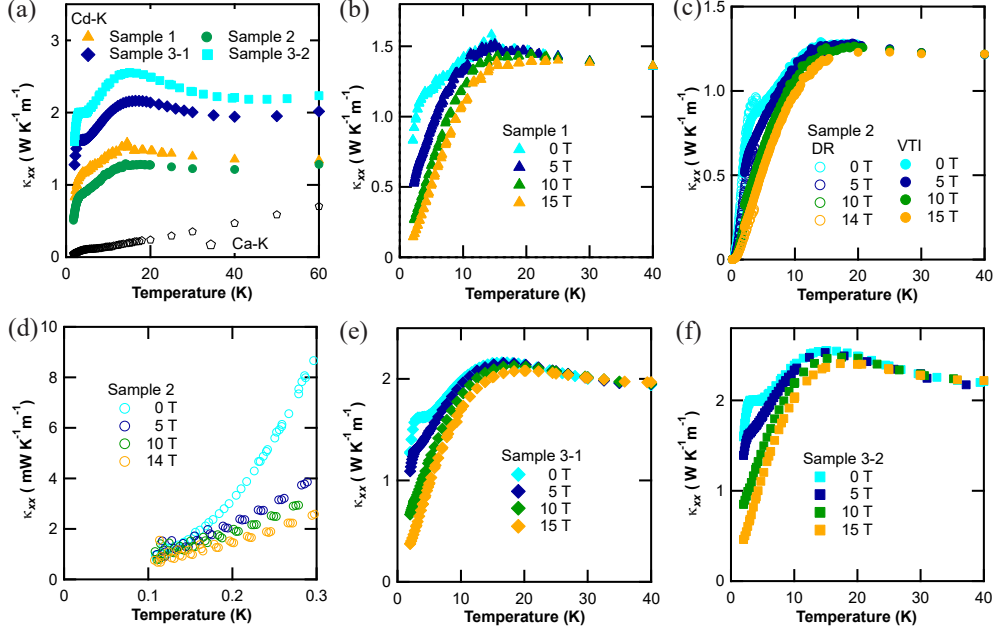


FIG. 2. (a) Temperature dependence of the longitudinal thermal conductivity (κ_{xx}) of all samples of Cd-Kapellasite (Cd-K) and that of Ca-Kapellasite (Ca-K) at 0 T. The longitudinal thermal conductivity of Ca-K is taken from Ref.¹⁹. (b to f) The data of each sample under magnetic fields. In the sample 2, κ_{xx} was measured down to 0.1 K. An enlarged view of low-temperature region (0.1–0.3 K) of (c) is shown in (d). The filled and open circles in (c) and (d) show κ_{xx} measured by a variable temperature insert (VTI) ($2 \text{ K} < T$) and a dilution refrigerator (DR) ($0.1 < T < 4 \text{ K}$), respectively.

field suppression effect is larger for a sample with a large κ_{xx} . The hump in the temperature dependence of κ_{xx} was observed at lower temperatures as the magnetic field was increased, implying a suppression of the magnetic transition temperature to lower temperatures (see Fig. 3).

Figure 4 shows the magnetic field dependence of κ_{xx} of sample 2. The vertical axis is normalized by the zero-field value as $[\kappa_{xx}(B) - \kappa_{xx}(0)]/\kappa_{xx}(0)$. The field dependence of κ_{xx} of other samples were essentially the same. Above 40 K, κ_{xx} increased linearly by applying the magnetic field (Fig. 4 (a)). On the other hand, below 30 K, the suppression of κ_{xx} by the magnetic field was observed (Fig. 4 (b)). The field suppression effect became larger at lower temperatures and reached the maximum reduction of $\sim 70\%$ by 15 T at 2 K. Below 0.3 K, a new peak was observed in the field dependence of κ_{xx} at 6–7 T (Fig. 4 (c)).

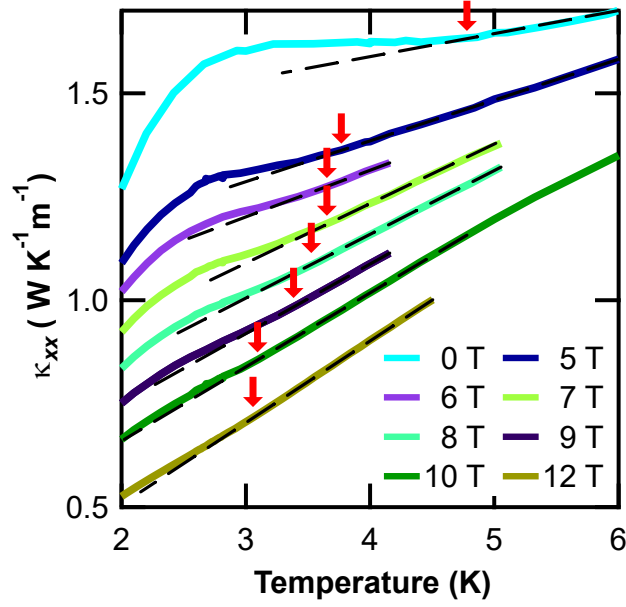


FIG. 3. Temperature dependence of κ_{xx} of Sample 3-1 near the Neel temperature at different fields. The red arrows point the field where κ_{xx} deviates from the linear temperature dependence (dash line) due to magnetic order.

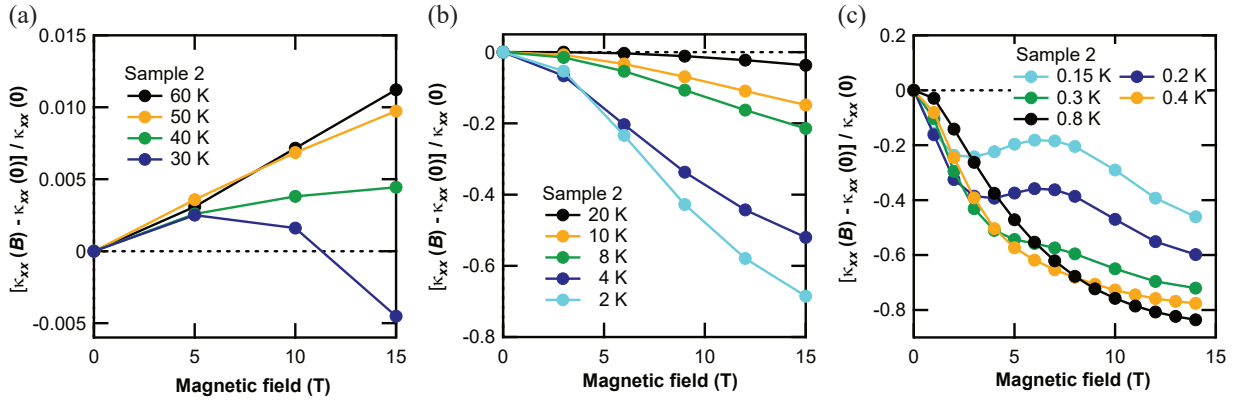


FIG. 4. Magnetic field dependence of the longitudinal thermal conductivity normalized by the zero field value ($[\kappa_{xx}(B) - \kappa_{xx}(0)]/\kappa_{xx}(0)$) of sample 2 above 30 K (a), for 2–20 K (b), and below 2 K (c).

B. Thermal Hall Conductivity

Figure 5(a) shows the magnetic field dependence of $\Delta T_y/Q$ of Sample 2 in the spin liquid phase. As shown in Fig. 5(a), the field dependence of κ_{xx} is dominated by the symmetric longitudinal component caused by the misalignment effect. To extract the asymmetric thermal Hall effect, the

field dependence of $\Delta T_y/Q$ is antisymmetrized with respect to the field direction as $\Delta T_y^{\text{Asym}}(B) = (\Delta T_y(+B) - \Delta T_y(-B))/2$. The field dependence of $\Delta T_y^{\text{Asym}}(B)$ of sample 2 is shown in Fig. 5(b). As shown in Fig. 5(b), $\Delta T_y^{\text{Asym}}/Q$ shows a linear magnetic field dependence at high temperatures.

The field dependence of κ_{xy} is determined by ΔT_y^{Asym} in accordance with Eq. 1, and is plotted in Fig. 6. From this field dependence, κ_{xy}/TB is estimated by the linear fitting of κ_{xy} as shown by the solid lines in Fig. 6. As shown in Fig. 6, the linear field dependence of κ_{xy} observed at 20 K becomes non-linear at lower temperatures, resulting in a large error in estimating κ_{xy}/TB at lower temperatures.

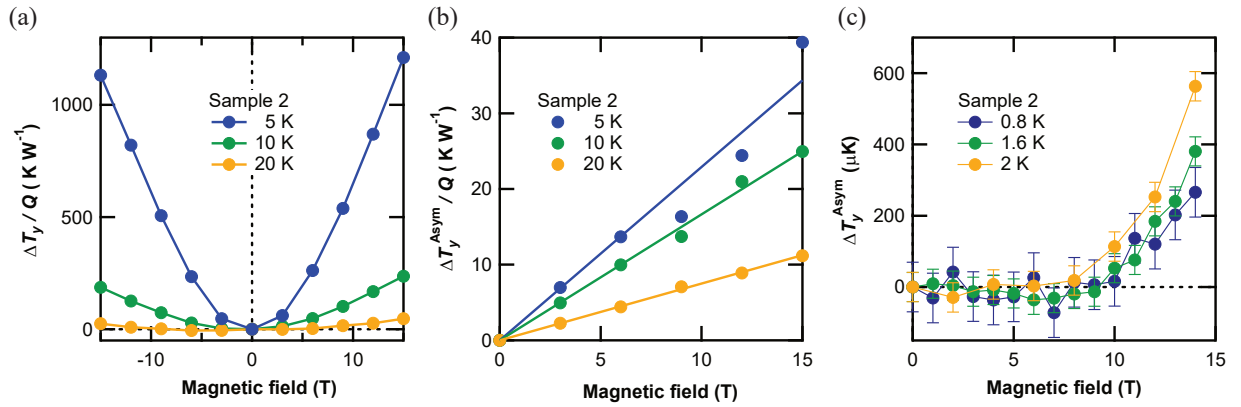


FIG. 5. (a) Magnetic field dependence of the transverse temperature difference divided by the heat current ($\Delta T_y/Q$). (b) Magnetic field dependence of asymmetric $\Delta T_y/Q$ of (a) with respect to the field direction. See text for details. The solid lines represent a linear fitting to $\Delta T_y^{\text{Asym}}/Q$ for each temperature. (c) Magnetic field dependence of $\Delta T_y^{\text{Asym}}/Q$ below 2 K. Error bars represent the standard deviation of the data.

This thermal Hall signal disappears in the AFM phase at low fields. Figure 5 (c) shows the field dependence of ΔT_y^{Asym} of sample 2 measured in a dilution refrigerator. As shown in Fig. 5 (c), the thermal Hall effect was absent at low fields, which is followed by an increase above ~ 7 T. Thus, for the measurements done in the dilution refrigerator, we determine κ_{xy}/TB by $\Delta T_y^{\text{Asym}}(B)$ at 14 T (open symbols in Fig. 8). A similar non-linear field dependence is confirmed in all Cd-K samples done at the lowest temperature of the VTI measurement (2 K) as shown in Fig. 7.

Figure 8 (a) shows the temperature dependence of the thermal Hall conductivity of all Cd-K samples. As shown in Fig. 8 (a), the thermal Hall conductivity κ_{xy}/TB of all Cd-K samples shows a similar temperature dependence with a peak around 8 K. In Sample 2, κ_{xy}/TB obtained in the ordered phase by the DR measurements is also shown by open symbols, which seems to be

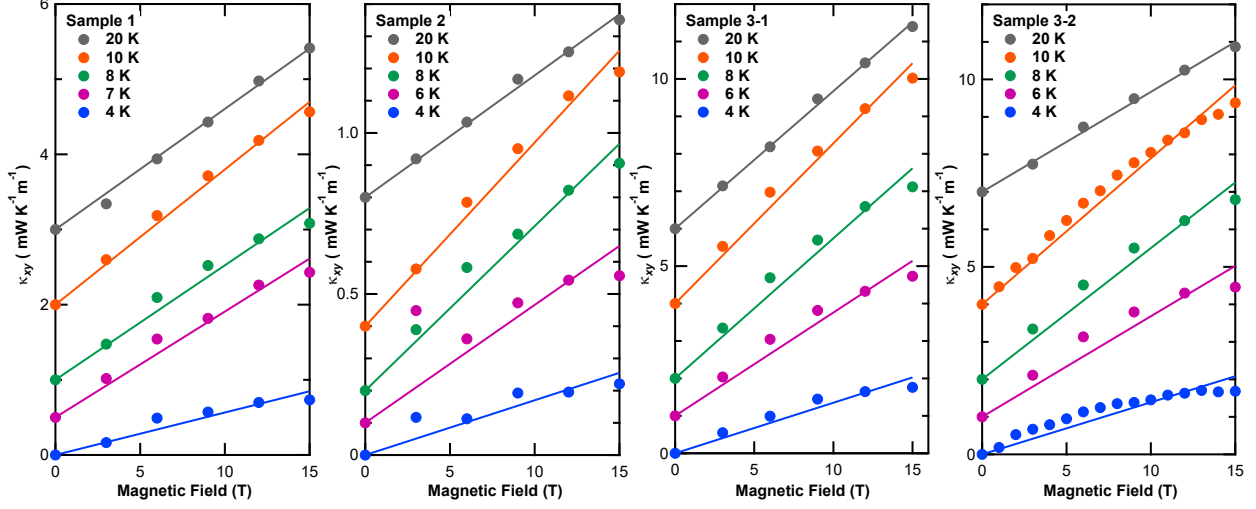


FIG. 6. The field dependence of κ_{xy} of all Cd-K samples for 4–20 K. The data above 4 K is shifted for clarity. The solid lines show a linear fit of the data to estimate κ_{xy}/TB at each temperatures.

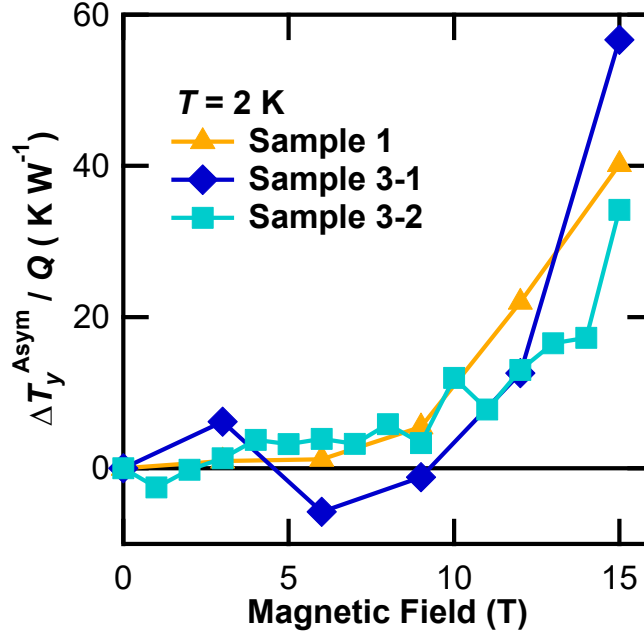


FIG. 7. Magnetic field dependence of the asymmetrized transverse temperature difference divided by the heat current ($\Delta T_y^{\text{Asym}}/Q$) at 2 K.

smoothly connected to the data measured by VTI (filled symbols). This temperature dependence is also similar to that of Ca-K¹⁹ and volborthite¹⁸ (Fig. 8 (b)). On the other hand, as shown in Fig. 8 (b), the peak temperature of κ_{xy}/TB is clearly shifted to a lower temperature in Cd-K.

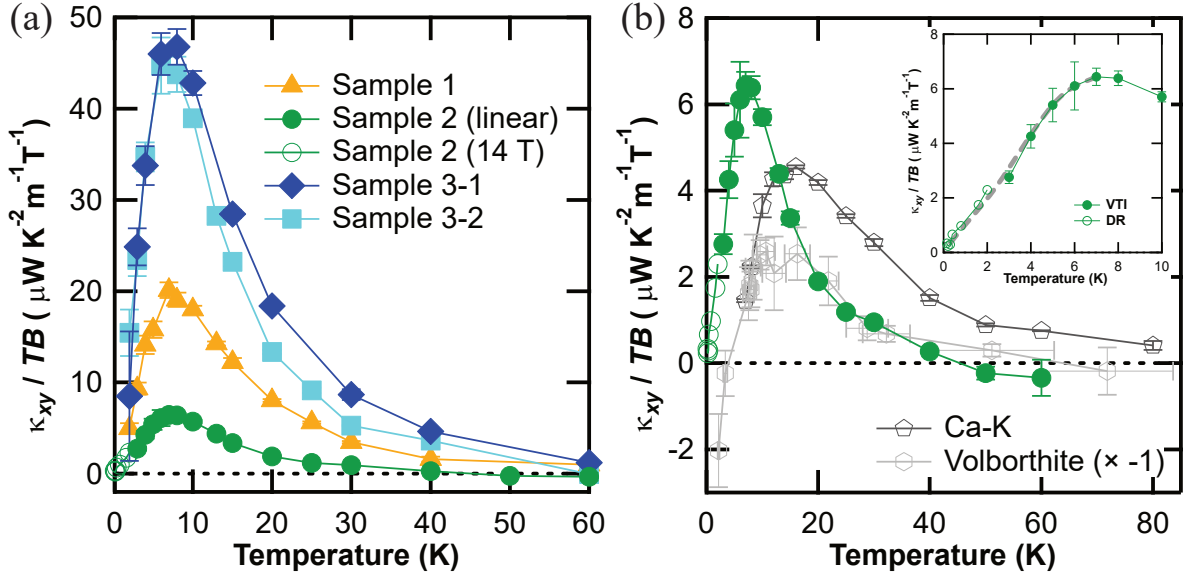


FIG. 8. Temperature dependence of κ_{xy}/TB . (a) Comparison of κ_{xy}/TB of three Cd-K samples. The filled (open) symbols represent κ_{xy}/TB calculated from the linear fitting of κ_{xy} in the VTI measurements (from the values at 14 T in the DR measurements). (b) Comparison of κ_{xy}/TB of Cd-K sample 2, Ca-K¹⁹ (open gray pentagon) and volborthite¹⁸ (open gray hexagon). For clarity, κ_{xy}/TB of volborthite is multiplied by -1 . Error bars corresponding to 1 standard deviation. The inset shows an enlarged view of the low temperature data of κ_{xy}/TB of sample 2. The dashed line shows a guide to the eye.

C. Specific Heat

Figure 9 (a) shows the temperature dependence of the specific heat (C) measured in multiple single crystals. The zero-field data shows a good agreement with the previous data⁴⁰ shown as open circles in Fig. 9. The specific heat under magnetic fields increases below 0.5 K owing to the nuclear Schottky anomaly (C_{Ncl}). The magnetic field dependence of the specific heat at 0.5 K is shown in Fig. 9 (b). After the specific heat was decreased by applying the magnetic field, the specific heat was increased by applying the magnetic field above 7 T. We note that this field increase of C above 7 T is much larger than that expected by C_{Ncl} (dotted line in Fig. 9 (b)) which is estimated as $\sim 2 \text{ mJ K}^{-1} \text{ mol}^{-1}$ at 0.5 K and 10 T from the fit of $C_{\text{Ncl}} \propto H^2/T^2$ for the data shown in Fig. 9 (a).

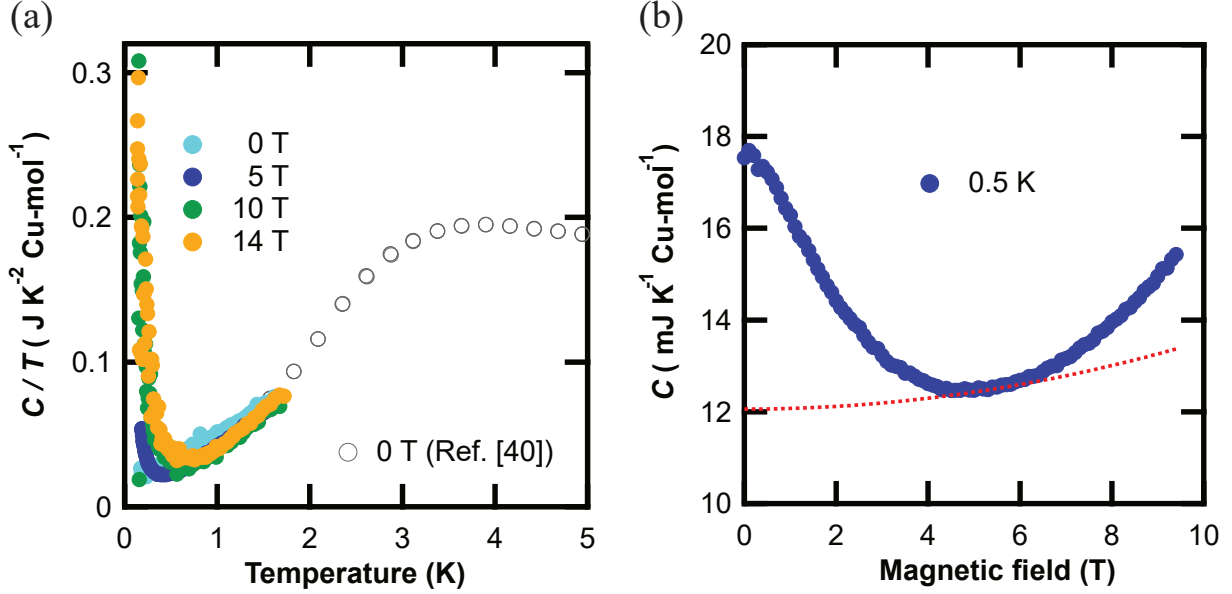


FIG. 9. (a) Temperature dependence of the specific heat divided by the temperature (C/T) measured in multiple single crystals. The zero-field data from the previous report⁴⁰ is also shown by open circles. (b) Magnetic field dependence of C at 0.5 K. The red dotted line shows an estimation of the magnetic field dependence of the nuclear Schottky specific heat (C_{Ncl}) at 0.5 K. The data of C_{Ncl} is shifted to compare the amount of the field increase.

IV. DISCUSSION

A. Longitudinal Thermal Conductivity

First, we discuss the sample dependence of κ_{xx} (Fig. 2 (a)) in terms of the sample quality. The longitudinal thermal conductivity of an insulator is given by the sum of the contribution of the phonons κ_{xx}^{ph} and that of the spins κ_{xx}^{sp} . Considering $J/k_B \sim 45$ K, it can be expected that κ_{xx} above 45 K is almost given by κ_{xx}^{ph} , which is consistent with the field dependence of κ_{xx} . It is known that κ_{xx}^{ph} increases in the magnetic field because the spin-phonon scatterings are reduced under magnetic field by suppressing spin fluctuations⁴⁴. In fact, as shown in Fig. 4 (a), the increase of κ_{xx} by applying the magnetic field is observed above 40 K, showing a dominant κ_{xx}^{ph} in κ_{xx} at high temperatures.

The phonon thermal conductivity κ_{xx}^{ph} is given by a product of the specific heat C_{ph} , the mean free path ℓ_{ph} , and the velocity v_{ph} of phonons, as $\kappa_{xx}^{\text{ph}} = (1/3)C_{\text{ph}}\ell_{\text{ph}}v_{\text{ph}}$. Since C_{ph} and v_{ph} are

common in all Cd-K samples, the difference in the magnitude of κ_{xx} shown in Fig. 2 (a) reflects the difference in ℓ_{ph} of each sample. Therefore, a sample with a larger κ_{xx} is a better crystal with less impurities. Also, the larger κ_{xx} of Cd-K than that of Ca-K shows that ℓ_{ph} of Cd-K is much longer than that of Ca-K because C_{ph} and v_{ph} of Cd-K are similar to those of the isostructural Ca-K. This longer ℓ_{ph} of Cd-K than that of Ca-K¹⁹ indicates that Cd-K has a more ideal kagome structure without the randomness of ions or the lattice defects found in Ca-K⁴⁵. We note that the difference of κ_{xx} of Sample 3-1 and that of Sample 3-2 might be caused by the ambiguity in estimating the sample size (up to 10%) owing to the irregular shape of the sample (see Fig. 1 (d)).

Next, we discuss the field suppression effect on κ_{xx} observed below 30 K (Fig. 4 (b)). One of the field-suppression mechanisms of κ_{xx}^{ph} , which normally increases in the magnetic field, is a resonance scattering of phonons being absorbed by impurity free spins⁴⁴. This resonant scattering is most effective when the spin Zeeman gap ($g\mu_B H$) coincides with the phonon peak ($\sim 4k_B T$) given by the Debye distribution, where μ_B is the Bohr magneton. Therefore, this resonance scattering produces a suppression peak of κ_{xx} at 5.4 T for 2 K as observed in volborthite¹⁸. However, as shown in Fig. 4(b), κ_{xx} at 2 K decreases monotonically with increasing magnetic field up to 15 T without the expected suppression peak. Therefore, the field suppression effect of κ_{xx} cannot be explained by the resonance scattering effect on κ_{xx}^{ph} . Therefore, the field suppression effect is caused by the decrease of κ_{xx}^{sp} under magnetic fields. A similar field suppression effect on κ_{xx}^{sp} has also been observed in the spin liquid state of the spin-chain compound⁴⁶, volborthite^{18,20} and Ca-K¹⁹. In volborthite, a field suppression effect up to $\sim 30\%$ at 15 T was observed²⁰ together with the resonance scattering effect¹⁸. Compared to the field suppression effects in volborthite and Ca-K, the field suppression of κ_{xx} in Cd-K is much larger (more than 70% at 2 K), showing a dominant contribution of κ_{xx}^{sp} in κ_{xx} at low temperatures.

Here, we consider the hump-like increase of κ_{xx} observed near T_N . This increase is caused by the increase of κ_{xx}^{ph} by a reduction of spin fluctuations⁴⁷ and/or the appearance of a magnon contribution in the ordered state²⁰. In the former case, as observed in $\alpha\text{-RuCl}_3$ (Ref.⁴⁷), the increase of κ_{xx} at T_N should be larger under higher fields because the spin fluctuations are more strongly suppressed under higher fields. However, as shown in Fig. 3, the increase becomes smaller at higher fields. This is consistent with the field suppression effect on κ_{xx}^{sp} . In addition, the large field suppression of κ_{xx} at low temperatures suggests a dominant contribution of κ_{xx}^{sp} . Therefore, the increase of κ_{xx} below T_N is likely attributed to the magnon contribution. The increase of κ_{xx} below T_N was observed larger in a better crystal with a larger κ_{xx} . We note that a similar sample depen-

dence of magnon thermal conduction has been observed in volborthite²⁰, which also supports the presence of a magnon contribution below T_N .

A new field-induced peak is observed in the magnetic field dependence of κ_{xx} around 7 T below 0.3 K (Fig. 4 (c)). Below 0.3 K, the resonance scattering effect on phonons takes place below 1 T. Also, the critical field of the AFM phase is much larger than 7 T because the hump-like increase of κ_{xx} is still observed above 7 T (Fig. 3). Therefore, this magnetic field dependence of κ_{xx} cannot be explained by an increase of κ_{xx}^{ph} by a reduction of the spin fluctuations. The magnon contribution is also excluded for the field-induced increase because the magnon contribution is suppressed by fields as observed as the decrease of the hump-like increase (Fig. 3). Therefore, this increase of κ_{xx} around 7 T indicates an appearance of some field-induced spin excitations.

The thermal conduction of spin is also given by $\kappa_{xx}^{\text{sp}} = C_{\text{sp}}v_{\text{sp}}\ell_{\text{sp}}/3$, where C_{sp} , v_{sp} , and ℓ_{sp} is the specific heat, the velocity and the mean free path of the spin excitations, respectively. As shown in Fig. 9 (b), the increase of C_{sp} is also observed around 7 T. This also supports the appearance of the field-induced excitations. Further, in the ordered phase, a finite thermal Hall effect is observed only above 7 T (Fig. 5 (c)), implying that the thermal Hall effect is caused by the field-induced excitations observed in the field dependence of κ_{xx} and C . As shown in Figs. 8, κ_{xy}/TB observed in the ordered phase above 7 T shows a good agreement with the data in the spin liquid phase, implying that the field-induced excitations in the ordered phase are similar to those in the spin liquid phase. This field dependence of the thermal Hall effect in the ordered phase of Cd-K is in sharp contrast to that observed in Ca-K¹⁹ where a finite κ_{xy} in the ordered phase is observed only in a low-field and is absent above ~ 6 T. This difference implies a difference in the ordered state of Cd-K from that in Ca-K.

B. Thermal Hall Conductivity

We first discuss the temperature dependence of κ_{xy}/TB of all three kagome compounds of Cd-K, Ca-K¹⁹, and volborthite¹⁸. As shown in Fig. 8 (b), κ_{xy}/TB of these kagome antiferromagnets shows a similar temperature dependence. As reported in Ref. 19, both the temperature dependence and the magnitude of κ_{xy}/TB of Ca-K and volborthite show a good agreement with a simulation based on the SBMFT^{25,48}. In the SBMFT framework, the kagome Heisenberg Hamiltonian with a Zeeman term and a DM interaction is diagonalized by taking a mean-field value of the bond operator of Schwinger bosons. From the energy bands and the Berry curvature calculated by the

SBMFT, $\kappa_{xy}^{\text{SBMFT}}$ is calculated by Eq. 1 and is expressed by a dimensionless function f_{SBMFT} as

$$\frac{\kappa_{xy}^{\text{SBMFT}}}{T} = \frac{k_B^2}{\hbar} \frac{Dg\mu_B B}{J^2} f_{\text{SBMFT}} \left(\frac{k_B T}{J} \right). \quad (3)$$

To compare this SBMFT calculation, the thermal Hall conductivity per one 2D kagome layer is estimated from the experimental data by $\kappa_{xy}^{2D} = \kappa_{xy} d$, where d ($d = 7.0328 \text{ \AA}$ for Cd-K⁴⁰) is the distance between the kagome layers. We then compare κ_{xy}^{2D} with f_{SBMFT} by normalizing κ_{xy}^{2D} as

$$\frac{\kappa_{xy}^{2D}}{T} = \frac{k_B^2}{\hbar} \frac{Dg\mu_B B}{J^2} f_{\text{exp}}, \quad (4)$$

where J and D are the fitting parameters.

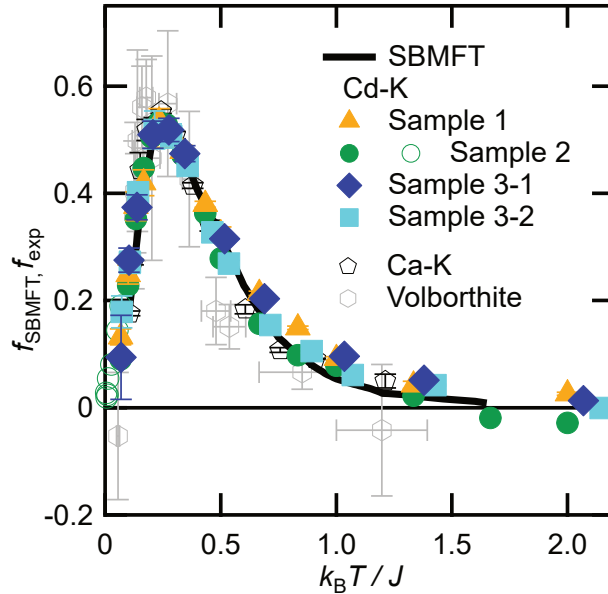


FIG. 10. Normalized thermal Hall conductivity f_{exp} of kagome lattice antiferromagnets fitted by the parameters listed in Table I. The solid line shows a numerical calculation of f_{SBMFT} at $D/J = 0.1$ by the Schwinger-boson mean field theory (SBMFT)¹⁹. The data of Ca-K and that of volborthite is taken from Ref. 19 and Ref. 18, respectively.

We have adopted this analysis for Cd-K and fitted κ_{xy}^{2D} by tuning the fitting parameters of J and D . Figure 10 shows the results of the fitting by the fitting parameters listed in Table I. As shown in Fig. 10, all the data well converges to one single curve given by the SBMFT (solid line in Fig. 10). However, $J = 30 \text{ K}$ used for the fit of Cd-K is considerably smaller than that estimated by the temperature dependence of χ ($J = 45 \text{ K}$)⁴¹. More importantly, the magnitude of D used to

TABLE I. Values of J and $|D/J|$ used to fit κ_{xy}^{2D} to the SBMFT simulation (Fig. 10) for kagome lattice antiferromagnets. The data of Ca-K and that of volborthite is taken from Ref. 19 and Ref. 18, respectively.

Material	Sample No.	J/k_B (K)	D/J
Cd-Kapellasite	1	30	0.28
	2	30	0.09
	3-1	29	0.65
	3-2	28	0.6
Ca-Kapellasite ¹⁹		66	0.12
Volborthite ¹⁸		60	-0.07

the fit of κ_{xy} of Cd-K differs in a factor of 7 among the Cd-K samples owing to the very different magnitudes of κ_{xy} . This large difference of D in Cd-K samples is too large to explain it by the ambiguity in estimating the sample dimensions. In addition, the largest value of $D/J = 0.65$ is unphysically larger than the value of $D/J \sim 0.19$ estimated from the deviation of the g factor from 2^{41} , This is in sharp contrast to the analysis done for Ca-K¹⁹ in which both J and D determined by the SBMFT fit of κ_{xy} well coincide with the value estimated from the temperature dependence of χ and that from the deviation of the g factor, respectively. These results indicate that the origin of the thermal Hall effect in Cd-K is different from the spin thermal Hall effect observed in Ca-K¹⁹.

To investigate the mechanism of the thermal Hall effect in Cd-K, we check the dependence of the maximum of $|\kappa_{xy}^{2D}|/TB$ on κ_{xx}/T at the peak temperature of $|\kappa_{xy}^{2D}|/TB$ for Cd-K, Ca-K and volborthite (Fig. 11). As shown in Fig. 11, the maximum of $|\kappa_{xy}^{2D}|/TB$ is looked constant for $\kappa_{xx}/T < 0.15 \text{ W K}^{-2} \text{ m}^{-1}$, which is followed by a linear increase for $\kappa_{xx}/T > 0.15 \text{ W K}^{-2} \text{ m}^{-1}$. This κ_{xx} dependence bears similarity to that of the anomalous Hall effect (AHE) in ferromagnetic metals. In the AHE, it has been known that the dominant mechanism of AHE depends on the magnitude of the longitudinal conductivity^{49,50}; the intrinsic mechanism by the Berry curvature of the energy bands is dominant in a moderate dirty metal whereas the extrinsic mechanism by skew scatterings is dominant for a super-clean metal. This good analogy between the thermal Hall effect in the kagome materials and the AHE in ferromagnetic metals implies a presence of another mechanism and/or carriers for the thermal Hall effect in a good insulator.

In the AHE in ferromagnetic metals, both the longitudinal and the transverse conduction are carried by electrons. In contrast, κ_{xx} of Cd-K is given by a sum of κ_{xx}^{ph} and κ_{xx}^{sp} . Therefore, κ_{xy} of

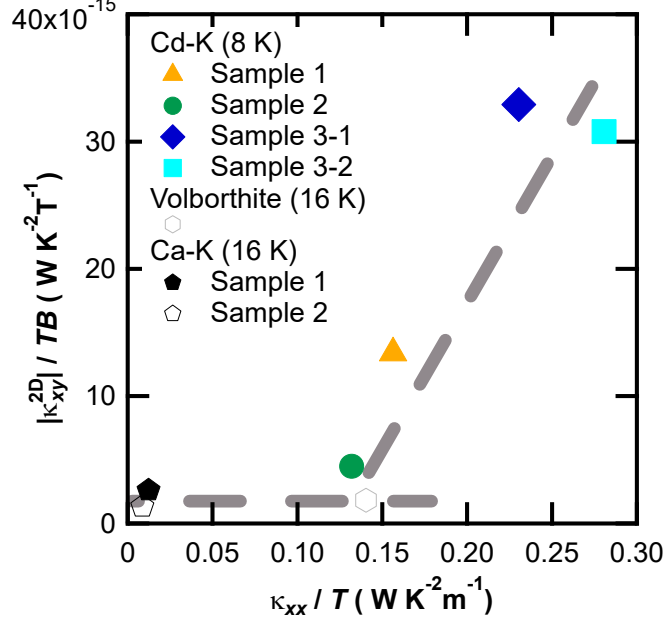


FIG. 11. The maximum of the thermal Hall conductivity of the 2D kagome layer $|\kappa_{xy}^{2D}|/TB$ of Cd-K and those of Ca-K¹⁹ and volborthite¹⁸ plotted as a function of the longitudinal thermal conductivity at the peak temperature of $|\kappa_{xy}^{2D}|/TB$ (8 K for Cd-K and 16 K for Ca-K and volborthite).

Cd-K can also be given a phonon contribution κ_{xy}^{ph} in addition to the spin contribution κ_{xy}^{sp} which is given by the SBMFT for Ca-K. As discussed in section IV A, a larger κ_{xx} of Cd-K reflects a larger κ_{xx}^{ph} given by a longer ℓ_{ph} in a better-quality sample. We therefore, from the positive correlation between κ_{xy} and κ_{xx} observed in Cd-K (Fig. 11), tentatively conclude that an *extrinsic* part of the thermal Hall conduction in Cd-K is phonon-mediated.

Thermal Hall effects of phonons has been reported in various compounds^{26–30}. In the nonmagnetic insulator SrTiO₃, in which only phonons are responsible for the thermal transport, κ_{xy} of phonons is found to show a peak at the same temperature of the peak in κ_{xx} . We thus checked this relation for Cd-K. In Cd-K, κ_{xx} of Cd-K contains a spin contribution κ_{xx}^{sp} which becomes dominant at lower temperatures. On the other hand, as shown in Fig. 4, a magnetic field suppresses a large portion of κ_{xx}^{sp} whereas it slightly increases κ_{xx}^{ph} . Therefore, κ_{xx}^{ph} can be estimated by κ_{xx} at 15 T.

Figure 12 shows the temperature dependence of κ_{xx}/T at 15 T (left axis) and that of κ_{xy}/T (right axis) of all Cd-K samples. As shown in Fig. 12, κ_{xx}/T at 15 T shows a peak at almost the same temperature of the peak of κ_{xy}/T , which resembles the case of the phonon thermal Hall effect observed in SrTiO₃ (Ref.²⁹). Therefore, this temperature dependence showing a peak at a similar

temperature indicates that κ_{xy} of Cd-K contains a dominant phonon contribution. We also find that this is clearly not the case for Ca-K. As shown in Figs. 12(e) and (f), κ_{xx}/T at 15 T peaks at a much lower temperature than that of κ_{xy}/T , which is consistent with the spin origin of κ_{xy} in Ca-K.

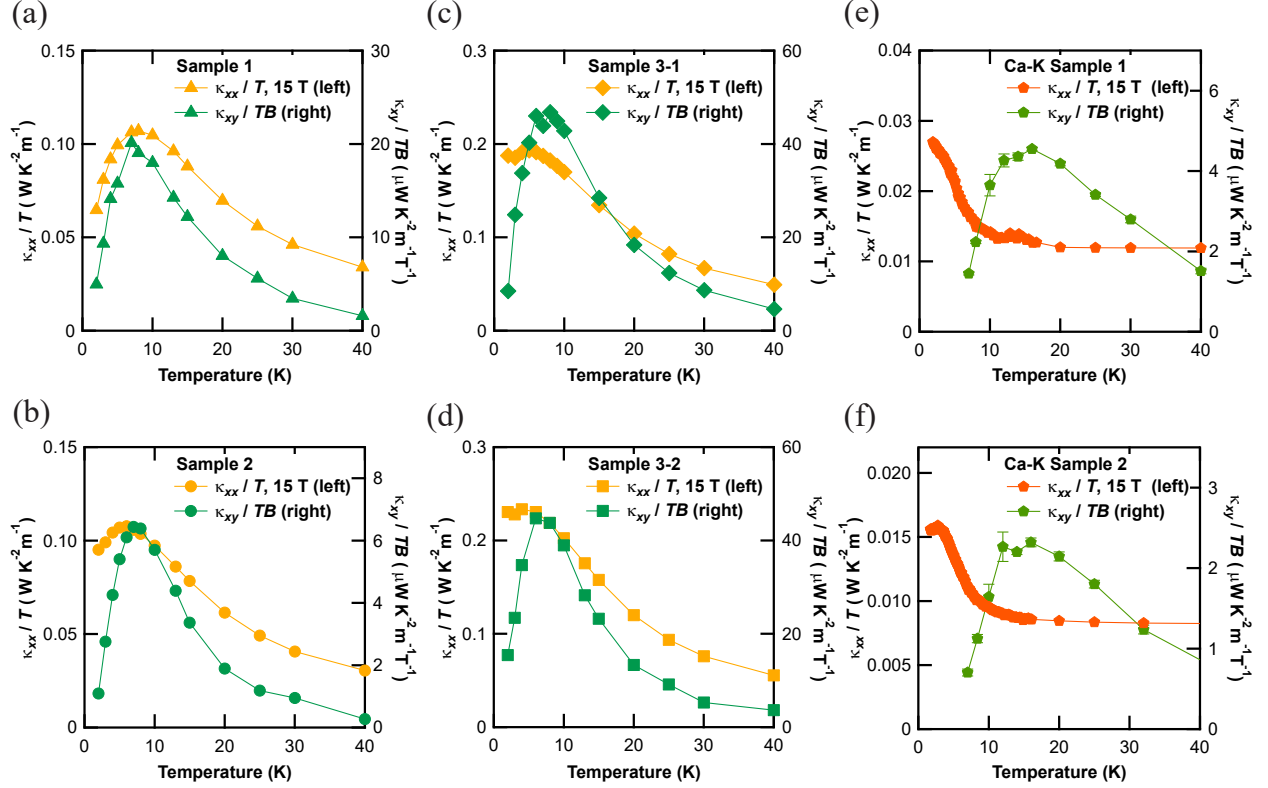


FIG. 12. Temperature dependence of κ_{xx}/T at 15 T (left axis) and that of κ_{xy}/T (right axis) of all Cd-K samples (a–d), and Ca-K (e, f). The data of Ca-K is taken from Ref. 19.

The energy scale of the phonon thermal Hall effect should be given by the Debye temperature, which is 180 K for Cd-K. Since this energy scale is order of magnitude larger than that of magnetic field of 15 T, κ_{xy}^{ph} is expected to have a linear field dependence. On the other hand, as shown in Fig. 6, κ_{xy} at low temperatures shows a non-linear field dependence that the slope of κ_{xy}/B is larger at lower fields. As discussed in section IV A, κ_{xx}^{sp} shows a similar field suppression effect which becomes larger at lower temperatures. Therefore, the non-linear field dependence of κ_{xy} suggests a presence of a spin contribution κ_{xy}^{sp} which is related to κ_{xx}^{sp} . We thus conclude that the thermal Hall effect in Cd-K contains both κ_{xy}^{ph} and κ_{xy}^{sp} , and that κ_{xy}^{sp} becomes larger at lower temperatures as κ_{xx}^{sp} does.

In the AFM phase of Cd-K, no thermal Hall effect is observed below ~ 7 T (Fig. 5(c)), showing

that both κ_{xy}^{ph} and κ_{xy}^{sp} disappear in the AFM phase at low fields. This field dependence is quite different from that of Ca-K¹⁹ where κ_{xy}^{sp} is observed only below ~ 6 T. This contrasting field dependence of κ_{xy}^{sp} in Cd-K implies that the ordered state in Cd-K has a different magnon spectrum from that of Ca-K, possibly by the larger D in Cd-K.

The temperature dependence of the high-field κ_{xy} below T_N well follows that at the spin liquid phase (the inset of Fig. 8(b)). Given that κ_{xy}^{ph} is dominant at 15 T, this high-field κ_{xy} below T_N is also given by phonons. Therefore, the field dependence of κ_{xy} in the AFM phase (Fig. 5(c) and Fig. 7) shows that the linear field dependence of κ_{xy}^{ph} disappears at low fields whereas it comes back at high fields. This absence of κ_{xy}^{ph} in the low-field AFM phase demonstrates that the phonons cannot alone exhibit the thermal Hall effect, putting a strong constraint on the origin of the phonon Hall effect. In other words, κ_{xy}^{ph} requires the field-induced excitations observed in the field dependence of κ_{xx} (Fig. 4(c)) and that of C (Fig. 9(b)).

Thermal Hall effects by phonons have been theoretically studied with respect to various aspects^{31–39}. The absence of the stand-alone phonon thermal Hall effect in Cd-K is inconsistent with intrinsic mechanism, but rather points to extrinsic origins with microscopic couplings between phonons and the field-induced excitations. Such microscopic coupling has also been suggested to play an important role in the thermal Hall effect observed in multiferroics⁵¹ where a large thermal Hall effect is observed in the ferrimagnetic phase despite the absence of the conventional magnon Hall effect. It has been pointed out that a magnon-phonon coupling induces a thermal Hall effect even in the system where neither phonons nor magnons alone show a thermal Hall effect³⁸. Therefore, the absence and the presence of κ_{xy}^{ph} in the AFM phase of Cd-K suggests that the phonon thermal Hall effect in Cd-K has an extrinsic origin requiring a coupling with the field-induced excitations. At present, the details of the magnetic structure of Cd-K have not been known. Further studies, including NMR or neutron scattering experiments to clarify the magnetic excitations in the AFM phase under the low and the high magnetic fields, will be important to reveal the origins of the thermal Hall effects in Cd-K.

One clearly has to wonder why, despite the dual origin (spins and phonons) of the thermal Hall effects in the Cd-K compounds, the scaling fit derived entirely from the SBMFT works so well as shown in Fig. 10. This is not an unreasonable conclusion, however, provided we further assume that κ_{xy}^{sp} is proportional to κ_{xy}^{ph} , due to the fact that the two excitations are microscopically coupled.

V. SUMMARY

We have investigated κ_{xx} and κ_{xy} of three Cd-K samples. From the large field suppression effect on κ_{xx} at low temperatures, we find a dominant contribution of κ_{xx}^{sp} in κ_{xx} at low temperatures. Below T_N , we find a new peak in the field dependence of κ_{xx} at ~ 7 T. Above 7 T, we also find a field-induced increase both in the specific heat and in the thermal Hall effect.

Clear thermal Hall effects have been observed in the spin liquid states of all Cd-K samples. We find that the temperature dependence of κ_{xy} shows a very similar temperature dependence with a peak at almost the same temperature. On the other hand, the magnitude of κ_{xy} depends on κ_{xx} . This κ_{xx} dependence is inconsistent with the spin thermal Hall effect observed in the related compound in Ca-K. We conclude that a phonon thermal Hall κ_{xy}^{ph} contributes to κ_{xy} of all Cd-K from the positive correlation between κ_{xy} and κ_{xx} (Fig. 11) and the similar temperature dependence of κ_{xy} and κ_{xx} at 15 T (Fig. 12). We further find that the non-linear field dependence of κ_{xy} at low temperatures (Fig. 6) shows the presence of a spin thermal Hall κ_{xy}^{sp} at low temperatures and at low fields. These results demonstrate that the spin liquid state of Cd-K harbors thermal Hall effects of both spins and phonons.

Remarkably, both κ_{xy}^{ph} and κ_{xy}^{sp} disappear in the AFM phase at low fields. At high fields above 7 T, we find that κ_{xy}^{ph} is induced concomitantly with the field induced excitations observed in the field dependence of κ_{xx} and C . These results suggest that field-induced excitations give rise to a recovery of the phonon thermal Hall effect of Cd-K. We conclude that the phonons alone do not exhibit the thermal Hall effect and require to merge with the field-induced excitations to appear.

ACKNOWLEDGMENTS

This work was supported by Grants-in-Aid for Scientific Research (KAKENHI) (No. 19H01809, No. 19H01848, and No. 19K21842).

* my@issp.u-tokyo.ac.jp

¹ S. Yan, D. A. Huse, and S. R. White, *Science* **332**, 1173 (2011).

² S. Depenbrock, I. P. McCulloch, and U. Schollwöck, *Physical Review Letters* **109**, 067201 (2012).

³ H.-C. Jiang, Z. Wang, and L. Balents, *Nature Physics* **8**, 902 (2012).

- ⁴ Y. Iqbal, F. Becca, S. Sorella, and D. Poilblanc, *Physical Review B* **87**, 060405 (2013).
- ⁵ S. Nishimoto, N. Shibata, and C. Hotta, *Nature Communications* **4**, 2287 (2013).
- ⁶ H. J. Liao, Z. Y. Xie, J. Chen, Z. Y. Liu, H. D. Xie, R. Z. Huang, B. Normand, and T. Xiang, *Physical Review Letters* **118**, 137202 (2017).
- ⁷ Y.-C. He, M. P. Zaletel, M. Oshikawa, and F. Pollmann, *Physical Review X* **7**, 031020 (2017).
- ⁸ S. Jiang, P. Kim, J. H. Han, and Y. Ran, *SciPost Phys.* **7**, 6 (2019).
- ⁹ S. Sachdev, *Physical Review B* **45**, 12377 (1992).
- ¹⁰ F. Wang and A. Vishwanath, *Physical Review B* **74**, 174423 (2006).
- ¹¹ L. Messio, S. Bieri, C. Lhuillier, and B. Bernu, *Physical Review Letters* **118**, 267201 (2017).
- ¹² D. E. Freedman, T. H. Han, A. Prodi, P. Müller, Q.-Z. Huang, Y.-S. Chen, S. M. Webb, Y. S. Lee, T. M. McQueen, and D. G. Nocera, *Journal of the American Chemical Society* **132**, 16185 (2010).
- ¹³ H. Katsura, N. Nagaosa, and P. A. Lee, *Physical Review Letters* **104**, 066403 (2010).
- ¹⁴ R. Matsumoto, R. Shindou, and S. Murakami, *Physical Review B* **89**, 054420 (2014).
- ¹⁵ Y. Onose, T. Ideue, H. Katsura, Y. Shiomi, N. Nagaosa, and Y. Tokura, *Science* **329**, 297 (2010).
- ¹⁶ T. Ideue, Y. Onose, H. Katsura, Y. Shiomi, S. Ishiwata, N. Nagaosa, and Y. Tokura, *Physical Review B* **85**, 134411 (2012).
- ¹⁷ M. Hirschberger, R. Chisnell, Y. S. Lee, and N. P. Ong, *Phys. Rev. Lett.* **115**, 106603 (2015).
- ¹⁸ D. Watanabe, K. Sugii, M. Shimozawa, Y. Suzuki, T. Yajima, H. Ishikawa, Z. Hiroi, T. Shibauchi, Y. Matsuda, and M. Yamashita, *Proceedings of the National Academy of Sciences* **113**, 8653 (2016).
- ¹⁹ H. Doki, M. Akazawa, H.-Y. Lee, J. H. Han, K. Sugii, M. Shimozawa, N. Kawashima, M. Oda, H. Yoshida, and M. Yamashita, *Physical Review Letters* **121**, 097203 (2018).
- ²⁰ M. Yamashita, M. Akazawa, M. Shimozawa, T. Shibauchi, Y. Matsuda, H. Ishikawa, T. Yajima, Z. Hiroi, M. Oda, H. Yoshida, H.-Y. Lee, J. H. Han, and N. Kawashima, *Journal of Physics: Condensed Matter* **32**, 074001 (2020).
- ²¹ M. Hirschberger, J. W. Krizan, R. J. Cava, and N. P. Ong, *Science* **348**, 106 (2015).
- ²² Y. Kasahara, K. Sugii, T. Ohnishi, M. Shimozawa, M. Yamashita, N. Kurita, H. Tanaka, J. Nasu, Y. Motome, T. Shibauchi, and Y. Matsuda, *Physical Review Letters* **120**, 217205 (2018).
- ²³ Y. Kasahara, T. Ohnishi, Y. Mizukami, O. Tanaka, S. Ma, K. Sugii, N. Kurita, H. Tanaka, J. Nasu, Y. Motome, T. Shibauchi, and Y. Matsuda, *Nature* **559**, 227 (2018).
- ²⁴ R. Hentrich, M. Roslova, A. Isaeva, T. Doert, W. Brenig, B. Büchner, and C. Hess, *Physical Review B* **99**, 085136 (2019).

- ²⁵ H. Lee, J. H. Han, and P. A. Lee, *Physical Review B* **91**, 125413 (2015).
- ²⁶ C. Strohm, G. L. J. A. Rikken, and P. Wyder, *Phys. Rev. Lett.* **95**, 155901 (2005).
- ²⁷ K. Sugii, M. Shimozawa, D. Watanabe, Y. Suzuki, M. Halim, M. Kimata, Y. Matsumoto, S. Nakatsuji, and M. Yamashita, *Phys. Rev. Lett.* **118**, 145902 (2017).
- ²⁸ Y. Hirokane, Y. Nii, Y. Tomioka, and Y. Onose, *Phys. Rev. B* **99**, 134419 (2019).
- ²⁹ X. Li, B. Fauqué, Z. Zhu, and K. Behnia, *Phys. Rev. Lett.* **124**, 105901 (2020).
- ³⁰ G. Grissonnanche, S. Thériault, A. Gourgout, M. E. Boulanger, E. Lefrançois, A. Ataei, F. Laliberté, M. Dion, J. S. Zhou, S. Pyon, T. Takayama, H. Takagi, N. Doiron-Leyraud, and L. Taillefer, *arXiv:2003.00111* (2020).
- ³¹ L. Sheng, D. N. Sheng, and C. S. Ting, *Phys. Rev. Lett.* **96**, 155901 (2006).
- ³² Y. Kagan and L. A. Maksimov, *Phys. Rev. Lett.* **100**, 145902 (2008).
- ³³ J.-S. Wang and L. Zhang, *Phys. Rev. B* **80**, 012301 (2009).
- ³⁴ L. Zhang, J. Ren, J.-S. Wang, and B. Li, *Phys. Rev. Lett.* **105**, 225901 (2010).
- ³⁵ T. Qin, J. Zhou, and J. Shi, *Phys. Rev. B* **86**, 104305 (2012).
- ³⁶ M. Mori, A. Spencer-Smith, O. P. Sushkov, and S. Maekawa, *Physical Review Letters* **113**, 265901 (2014).
- ³⁷ T. Saito, K. Misaki, H. Ishizuka, and N. Nagaosa, *Phys. Rev. Lett.* **123**, 255901 (2019).
- ³⁸ X. Zhang, Y. Zhang, S. Okamoto, and D. Xiao, *Phys. Rev. Lett.* **123**, 167202 (2019).
- ³⁹ J.-Y. Chen, S. A. Kivelson, and X.-Q. Sun, *Phys. Rev. Lett.* **124**, 167601 (2020).
- ⁴⁰ R. Okuma, T. Yajima, D. Nishio-Hamane, T. Okubo, and Z. Hiroi, *Physical Review B* **95**, 094427 (2017).
- ⁴¹ R. Okuma, D. Nakamura, T. Okubo, A. Miyake, A. Matsuo, K. Kindo, M. Tokunaga, N. Kawashima, S. Takeyama, and Z. Hiroi, *Nature Communications* **10**, 1229 (2019).
- ⁴² M. P. Shores, E. A. Nytko, B. M. Bartlett, and D. G. Nocera, *Journal of the American Chemical Society* **127**, 13462 (2005).
- ⁴³ R. D. Shannon, *Acta Crystallographica A* **32**, 751 (1976).
- ⁴⁴ R. Berman, *Thermal Conduction in Solids*, Oxford Studies in Physics (Clarendon Press, Oxford, 1976).
- ⁴⁵ H. Yoshida, N. Noguchi, Y. Matsushita, Y. Ishii, Y. Ihara, M. Oda, H. Okabe, S. Yamashita, Y. Nakazawa, A. Takata, T. Kida, Y. Narumi, and M. Hagiwara, *Journal of the Physical Society of Japan* **86**, 033704 (2017).
- ⁴⁶ A. V. Sologubenko, K. Berggold, T. Lorenz, A. Rosch, E. Shimshoni, M. D. Phillips, and M. M. Turnbull, *Phys. Rev. Lett.* **98**, 107201 (2007).

- ⁴⁷ R. Hentrich, A. U. B. Wolter, X. Zotos, W. Brenig, D. Nowak, A. Isaeva, T. Doert, A. Banerjee, P. Lampen-Kelley, D. G. Mandrus, S. E. Nagler, J. Sears, Y.-J. Kim, B. Büchner, and C. Hess, *Phys. Rev. Lett.* **120**, 117204 (2018).
- ⁴⁸ J. H. Han and H. Lee, *Journal of the Physical Society of Japan* **86**, 011007 (2017).
- ⁴⁹ S. Onoda, N. Sugimoto, and N. Nagaosa, *Physical Review Letters* **97**, 126602 (2006).
- ⁵⁰ S. Onoda, N. Sugimoto, and N. Nagaosa, *Physical Review B* **77**, 165103 (2008).
- ⁵¹ T. Ideue, T. Kurumaji, S. Ishiwata, and Y. Tokura, *Nature Materials* **16**, 797 (2017).